Nanoscale groove textured β-Ga_2O_3 by room temperature inverse metal-assisted chemical etching and photodiodes with enhanced responsivity

Munho Kim, Hsien-Chih Huang, Jeong Dong Kim, Kelson D. Chabak, Akhil Raj Kumar Kalapala, Weidong Zhou, and Xiuling Li

Citation: Appl. Phys. Lett. **113**, 222104 (2018); doi: 10.1063/1.5053219
View online: https://doi.org/10.1063/1.5053219
View Table of Contents: http://aip.scitation.org/toc/apl/113/22
Published by the American Institute of Physics

Nanoscale groove textured β-Ga_2O_3 by room temperature inverse metal-assisted chemical etching and photodiodes with enhanced responsivity

Munho Kim,[1,a)] Hsien-Chih Huang,[1] Jeong Dong Kim,[1] Kelson D. Chabak,[2] Akhil Raj Kumar Kalapala,[3] Weidong Zhou,[3] and Xiuling Li[1,b)]
[1]*Department of Electrical and Computer Engineering, Micro and Nanotechnology Laboratory, Materials Research Laboratory, Institute of Carbon-Neutral Energy Research Institute, University of Illinois at Urbana-Champaign, Urbana, Illinois 61801, USA*
[2]*Air Force Research Laboratory, Sensors Directorate, Wright-Patterson AFB, Ohio 45433, USA*
[3]*Department of Electrical Engineering, University of Texas at Arlington, Arlington, Texas 76019, USA*

(Received 22 August 2018; accepted 9 November 2018; published online 30 November 2018)

β-Ga_2O_3 is an emerging wide band-gap semiconductor that holds great promise for next generation power electronics and optoelectronics. β-Ga_2O_3 based ultraviolet photodetectors have been the subject of active research for the last few years. However, no micro and nanostructure surface texturing has been demonstrated for efficient light management in β-Ga_2O_3 optoelectronic applications yet. We hereby present nanoscale groove textured β-Ga_2O_3 metal-semiconductor-metal photodiodes, enabled by the unique metal-assisted chemical etching (MacEtch) method at room temperature in liquid. Although the textured surface stoichiometry shows ~10% oxygen deficiency which results in a reduced Schottky barrier height and increased dark current, clear enhancement of the responsivity is demonstrated, compared to the planar untreated surface. The realization of MacEtch's applicability to β-Ga_2O_3 opens the door for producing more sophisticated device structures for this material, without resorting to conventional dry etch and potential damage. *Published by AIP Publishing.*
https://doi.org/10.1063/1.5053219

Photodetectors are one of the most important optoelectronic devices for optical sensing across various wavelength ranges. In many of these applications, it is highly desirable to detect UV light without sensing visible or IR light since false detection can happen due to the solar radiation with the wavelength longer than 280 nm.[1] For the III-N material system, $Al_xGa_{1-x}N$ alloys with a high concentration of Al ($x > 30\%$) are necessary to achieve a solar-blind cut-off wavelength.[2–6] This has met many technical challenges such as deterioration of epitaxially grown $Al_xGa_{1-x}N$ films, poor p-type doping, and residual strain.[7] Other wide band-gap (WBG) materials (e.g., BN, $LaAlO_3$, $In_2Ge_2O_7$, and diamond) are suitable for solar-blind UV photodetectors due to their intrinsic solar-blindness and low dark currents.[8–11] However, most of the fabrication processes for these materials are complex and expensive.

β-Ga_2O_3 is an emerging WBG material for applications in high power electronics and solar-blind UV photodetectors due to the band-gap energy of ~4.9 eV.[12] In addition, β-Ga_2O_3 has advantages over other WBG materials such as the availability of single crystalline bulk substrates and homoepitaxial growth capability with controllable n-type doping over the range of 10^{15}~10^{20} cm^{-3}.[12,13] So far, mainly two types [i.e., metal-semiconductor-metal (MSM) and vertical Schottky] of β-Ga_2O_3 photodetectors based on bulk substrates and thin films have been realized.[14,15] β-Ga_2O_3 nanowires and nanoflakes have also been employed to fabricate photodetectors.[16,17] Although overall good performance has been achieved from these devices, the use of anti-reflective (AR) structures on β-Ga_2O_3 has not yet been reported, presumably due to the difficulties in realizing proper AR structures on this material. AR structures are arrays of textures with dimensions smaller (sub-wavelength scale) or larger (surface-texture) than the wavelength of the incident light, which create a graded refractive index at the surface, reducing the amount of the reflected light and enhancing optical absorption. Efficient light management by this approach has been widely used in various semiconductor-based optoelectronic and photovoltaic devices for improving the absorption properties of the devices.[18] Note that various types of AR structures have been used showing the improvement of device performance of SiC photodetectors and GaN light emitting diodes (LEDs).[19,20] Recently, inductively coupled plasma reactive ion etching (ICP-RIE) of β-Ga_2O_3 has been studied to optimize the etch condition for surface roughness and etch rate.[21–23] It was found that the plasma-induced damage increases with the etch rate.[21] Yang *et al.* subsequently demonstrated that annealing at 450 °C effectively removes the damage.[22] Note that the surface examined after ICP-RIE was (-201) substrates and the damage on the sidewalls remains to be explored. To produce AR structures, a wet etching process is typically preferred over a dry etching because dry etching processes can result in non-repairable high-energy ion induced surface damages such as point defects which normally behave as recombination centers. Preliminary studies of wet etching of β-Ga_2O_3 have been reported back in 2008,[24,25] where an elevated temperature (120–150 °C) was mostly required, and its effect on the material quality has not been well characterized. Recently, photo-enhanced chemical (PEC) etching was used to tune the threshold via the channel thickness of an exfoliated (-201) Ga_2O_3 flake-based MOSFET.[26] However, PEC under a more controlled environment may be necessary, since the etching was carried out by immersing a fully fabricated MOSFET with metal contacts on both the front (source and drain) and

a)Present address: School of Electrical and Electronic Engineering, Nanyang Technological University, 50 Nanyang Avenue, 639798 Singapore, Singapore.
b)Author to whom correspondence should be addressed: xiuling@illinois.edu

back (gate) sides of the flakes sitting on SiO_2 into hot H_3PO_4 under 254 nm UV exposure.

Metal-assisted chemical etching (MacEtch), an anisotropic semiconductor wet etching method spatially defined by metal catalyst patterns,[27,28] has been used to produce device quality photonic and electronic 3D structures in Si,[29] Ge,[30] GaAs,[31] InP,[32,33] and InGaAs,[34] because of its simplicity, effectiveness, and versatility in the absence of high energy ion induced damage. Here, we report the realization of AR structures at room temperature by MacEtch consisting of nanoscale grooves on (010) β-Ga_2O_3 substrates for light absorption enhancement and the performance of a MSM photodiode. In addition, the MacEtch mechanism of β-Ga_2O_3 and the resulting surface and interface effect on the device performance are characterized and analysed.

Photoenhanced MacEtch of WBG materials has been demonstrated by using an appropriate catalyst (e.g., Pt), oxidant [e.g., potassium persulfate ($K_2S_2O_8$)], and an UV illumination source,[35] including GaN and SiC.[36,37] In this work, unintentionally doped (010) β-Ga_2O_3 substrates (Tamura) were patterned by standard photolithography following cleaning by acetone, isopropyl alcohol, and DI water. A 15 nm thick layer of Pt film was then e-beam evaporated on the patterned surface with a deposition rate of 0.2 Å/s followed by liftoff. The Pt patterns formed are arrays of squares of $3 \times 3\,\mu m^2$ and spaced by 2 μm. Arrays of these Pt squares were placed on the periphery of a $5 \times 5\,mm^2$ sample to achieve evenly distributed textures on the entire surface. The patterned samples were immersed in a mixture of hydrofluoric acid (HF, 49%) and $K_2S_2O_8$ with a molar concentration of 0.28 M and 0.18 mM, respectively, under the illumination of a 254 nm UV lamp (Raytech) for 5–10 h. The UV lamp-substrate distance was ~6 cm. The etched morphology was inspected by scanning electron microscopy (SEM, Hitachi S-4700) and atomic force microscopy (AFM, Digital Instruments Nanoscope IIIa Multimode) with Si cantilevers operating in the non-contact mode. Surface stoichiometry and band-gap energy of the planar and textured samples were measured by x-ray photoelectron spectroscopy (XPS, Kratos Axis ULTRA). Surface reflection spectra were recorded by a custom-built reflection measurement system in a wavelength range of 200~300 nm.[38] MSM photodiodes were fabricated on the planar and textured surfaces covered with nanoscale grooves. Interdigitated metal electrodes of Ti/Au (10/80 nm) with an 8 μm width, 26 μm spacing, and 290 μm length were e-beam evaporated on top surfaces. The current-voltage (I-V) characteristics of the devices were measured using a semiconductor parameter analyzer (Keithley 4200). The photoresponse of the photodiodes fabricated on the planar and textured surface was measured at 254 nm using a Raytech UV lamp.

Figure 1(a) shows the 45° tilted SEM images of β-Ga_2O_3 with an array of square mesa, produced using a discrete Pt square array catalyst pattern (the Pt catalyst was removed before SEM) after a nominal period of 10 h etching in a mixture of HF (0.28 M) and $K_2S_2O_8$ (0.18 mM) without replenishing the solution under UV irradiation (254 nm). The resulting square mesa height is about 1 μm. Importantly, under identical conditions, no etching has been observed at all without the presence of Pt metal, confirming the metal-assisted mechanism of this etching process. The areas underneath the Pt catalyst

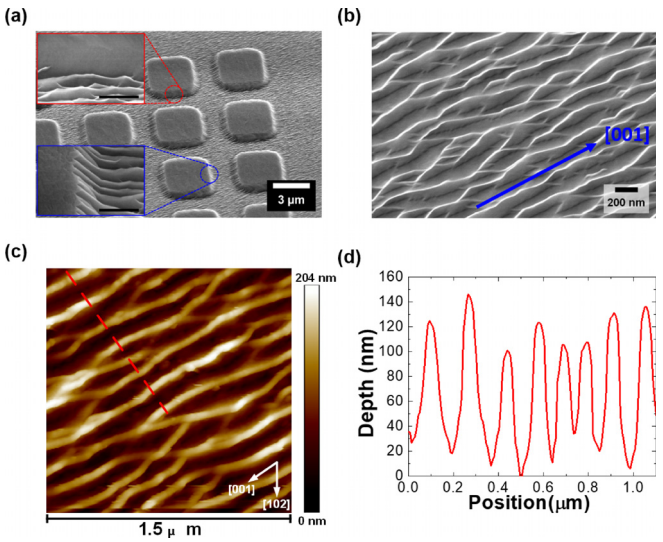

FIG. 1. Morphology of the β-Ga_2O_3 surface after 10 h of MacEtch under specified conditions. (a) 45° tilted SEM image of the area around a Pt square array catalyst pattern. The insets are zoomed-in SEM images of the sidewalls of the square mesa parallel (top) and perpendicular (bottom) to the grooves. The scale bar of the inset is 200 nm. (b) Top view SEM image of the region with the nanoscale groove textured surface. The [001] crystal orientation is indicated by the blue arrow. (c) 2D AFM image of the same region as in (b). (d) Cross-sectional depth analysis along the red scan line in (c).

were unetched except some undercut, while the areas around the catalyst were etched, reflecting the Inverse-MacEtch (I-MacEtch) nature.[30,32,33] Note that the metal functions as a catalyst in MacEtch so it does not get consumed. Because it is a room temperature process, no metal will diffuse into the body of the semiconductor. The catalyst metal can be removed before device processing. In the case of I-MacEtch where the metal remains on the surface, the metal can be removed readily by simple methods including blowing with a N_2 gun.

In contrast to other I-MacEtch examples reported previously,[30,32,33,39,40] the etched morphology reveals uniformly textured nanoscale grooves nearly aligned towards the same direction, identified to be along the [001] direction based on the substrate and wafer flat orientations. The insets in Figure 1(a) show zoomed-in SEM images of the sidewalls of the square mesa parallel (top) and perpendicular (bottom) to the grooves, respectively. The sidewalls perpendicular to the grooves are completely covered with the grooves that continue to propagate, while the mesa sidewalls parallel to the grooves are much smoother. Note that the sides of the square mesa in this case were intentionally aligned to the direction of the etched grooves, which does not change no matter how the Pt mesa is oriented. Figures 1(b) and 1(c) show the top view SEM and 2D AFM images of the propagating nanoscale grooves. Figure 1(d) shows the corresponding AFM line scan vertical profile, where the nanoscale grooves are approximately 120 and 150 nm in depth and width, respectively. The nominal vertical etch rate for the Pt covered mesa region is ~100 nm/h, while the etching spreads laterally across the entire wafer piece ($5 \times 5\,mm^2$) to form the shallow grooves. It is interesting that the shape and orientation of the etch pits formed on the initial stage of the I-MacEtch are similar to those as-grown (010) β-Ga_2O_3 single crystals reported by Hanada *et al.*[41] Note that the (100) plane is the energetically stable plane of β-Ga_2O_3[41] and the etch pits formed in the [001] direction leave some of the

(100) planes exposed on the sidewalls of these grooves. We hypothesize that the etch pits are enlarged as the etch time increases and then merged together to form the nanoscale grooves observed here.

Figure 2 illustrates the proposed I-MacEtch mechanism for β-Ga_2O_3, where electron (e^-) and hole (h^+) pairs are generated [Fig. 2(a)] by the above gap UV light, β-$Ga_2O_3 \xrightarrow{h\nu}$ β-$Ga_2O_3 + e^- + h^+$, in areas that are not covered by the Pt catalyst pattern. We hypothesize that in the HF-$K_2S_2O_8$ solution, β-Ga_2O_3 MacEtch can take place through the following chemical reactions [Eqs. (1)–(3)]. At the *Pt* catalyst surface (cathode), the oxidant ($K_2S_2O_8$) gets reduced [Eq. 1(a)], by consuming *e-* locally. Photo-pyrolysis of $S_2O_8^{2-}$ and subsequent reduction to SO_4^{2-} could also take place as described by Eqs. 1(b1) and 1(b2). Because of the nature of the localized holes, no oxidation reaction of β-Ga_2O_3 takes place underneath *Pt*. Instead, the photo-generated *e-* diffuses towards *Pt*, which causes excess photo-generated holes on the surface of β-Ga_2O_3 with no Pt [Fig. 2(b)]. The trapped holes induce oxidation reactions as described in Eq. 2(a), where Ga_2O_3 gets oxidized presumably to generate O_2 (bubbles observed). It is known that GaF_3 is insoluble in water, but it dissolves in HF [Eq. 2(b)], in which it forms an adduct with water ($GaF_3 \cdot H_2O$).[36]

Cathode reaction (at metal)

$$S_2O_8^{2-} + 2e^- \xrightarrow{Pt} 2SO_4^{2-}, \tag{1a}$$

$$S_2O_8^{2-} \xrightarrow{h\nu} 2SO_4^{-}, \tag{1b1}$$

$$SO_4^{-} + e^- \xrightarrow{Pt} SO_4^{2-}. \tag{1b2}$$

Anode reaction

$$Ga_2O_3 + 6h^+ \rightarrow 2Ga^{3+} + 3/2O_2, \tag{2a}$$

$$2Ga^{3+} + 6HF \rightarrow 2GaF_3 + 6H^+. \tag{2b}$$

Overall reaction

$$2Ga_2O_3 + 6S_2O_8^{2-} + 12HF \xrightarrow{h\nu, Pt} 4GaF_3 + 12SO_4^{2-} + 12H^+ + 3O_2 \uparrow . \tag{3}$$

The rate of I-MacEtch is known to be crystal orientation dependent[32] and for β-Ga_2O_3, I-MacEtch results in well-aligned nanoscale grooves along the [001] direction. Note that under the etch condition explored here, the etched sample is covered by the nano-groove texture, including those areas adjacent to the Pt square pads as shown in Fig. 1(a) and those that are remote (>1 mm) from them. Although the mechanism for the remote I-MacEtch, not widely observed for other MacEtch cases, is not completely clear at this point, it is likely related to the extremely slow etch rate and the localization of holes in this material. We believe the slow vertical etch rate in turn allows crystal-orientation to play a significant role and time for the lateral etch to take place even in areas remote from the catalyst. Here, we take advantage of the remote MacEtch phenomenon and fabricate MSM photodiodes on surfaces that are uniformly covered across the entire device area ($5 \times 5\,mm^2$) by the nanoscale grooves, simply by placing the Pt catalyst only on the edges and corners of the device sample.

The chemical composition of the β-Ga_2O_3 surface was examined by XPS. Figure 3(a) shows the XPS survey scan of β-Ga_2O_3 before and after the MacEtch process, as indicated. No change in the peak position was observed after MacEtch. The XPS spectra of O1s (~528.9 eV) and Ga2p (~1142.6 eV) peaks are shown in Figs. S2(a) and S2(b), from which the ratio of O1s and Ga2p peak intensities normalized to the stoichiometric value before etching is plotted in Fig. 3(b) as a function of etching time. The surface composition (O/Ga ratio) of β-Ga_2O_3 shows a decrease from ~1.47 to ~1.37 and ~1.32 after MacEtch for 5 and 10 h, respectively. This indicates that more oxygen is removed from β-Ga_2O_3 than Ga by the process of MacEtch, resulting in an oxygen deficient surface. The associated change in the band-gap of β-Ga_2O_3 was investigated by the energy loss spectra of O1s photoelectrons as shown in Figs. 3(c) and 3(d). The band-gap can be estimated by intercepting the linear extrapolation of the leading edge to the background level,[42] which is ~4.8 eV before etching, consistent with the reported value for β-Ga_2O_3,[43] and ~4.1 eV after MacEtch. The reduced band-gap after MacEtch should be the result of the oxygen deficiency. It was reported that the band-gap energy of oxygen deficient β-Ga_2O_x layers was reduced due to increased electron affinity.[44] Therefore, the Schottky barrier height (SBH) between the metal and etched β-Ga_2O_3 should be reduced. To determine the SBHs,

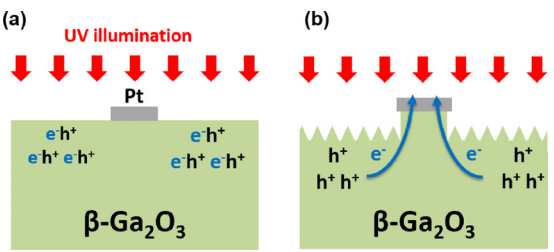

FIG. 2. Schematic illustration of the hypothesized I-MacEtch process that forms the nanoscale grooved textures: (a) Generation of electron (e^-) and hole (h^+) pairs in the β-Ga_2O_3 region not covered with Pt by 254 nm UV illumination. (b) Diffusion of photo-excited electrons towards the Pt catalyst by the reduction of the oxidant, leaving behind excess photo-excited holes to etch β-Ga_2O_3.

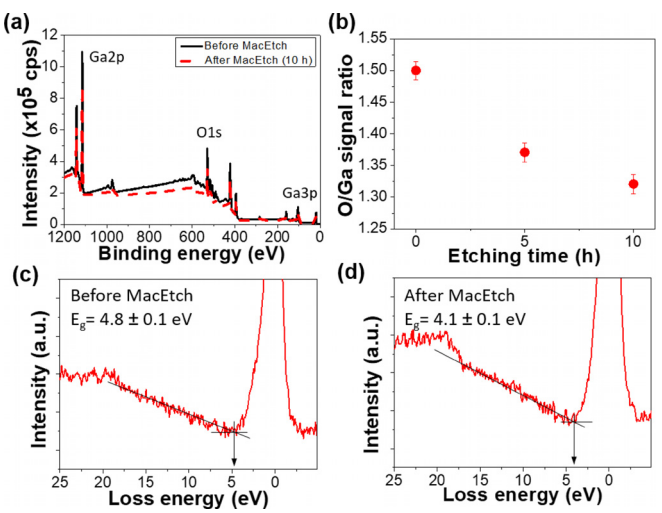

FIG. 3. XPS characterization of the β-Ga_2O_3 surface before and after MacEtch: (a) XPS survey scan. (b) O/Ga ratio as a function of etching time based on O1s and Ga2p peak intensity. (c) and (d) Energy loss spectra of O1s photoelectrons for β-Ga_2O_3. The band-gap energy is extracted by the intercept of the linear extrapolation of the leading edge to the background level.

the current-voltage characteristics under different temperatures were carried out on the samples with planar and textured surfaces (Fig. S3). For Schottky contacts, the current-voltage behavior above room temperature can be described by the thermionic emission equation[45]

$$I = AA^*T^2e^{-q\Phi_B/nkT}\left(e^{qV/nkT} - 1\right),$$

where q is the electron charge, A is the area of Schottky contact, A^* is the Richardson constant, and Φ_B is the SBH, n is the ideality factor, k is the Boltzmann constant, and T is the temperature. The Richardson constant of β-Ga_2O_3 is 33.61 A/cm^2 K^2.[46] The SBH can be extracted from the slope of $ln(I/T^2)$ *vs.* q/kT plot. Figure 4(a) shows the comparison of $ln(I/T^2)$ *vs.* q/kT at 0.5 V for the samples with planar and textured surfaces. The SBHs between Pt and β-Ga_2O_3 with the planar and textured surface were measured to be 1.49 and 1.36 eV, respectively. Note that the measured value between Pt and the planar surface agrees well with those in the literature.[46] The decrease in the SBH value between Pt and the textured surface is confirmed and attributed to the sub-oxide formation and thus the increased electron affinity of the textured surface. The correlation between SBH decrease and oxygen deficiency is further supported when the MacEtch time was extended using Pt strips to produce high aspect ratio fin arrays, which will be detailed in a future study.

Optical reflection occurs at semiconductor surfaces due to the difference in the refractive index between air and the semiconductor. This effect is one of the most important factors to determine the photoresponse of optoelectronic and photovoltaic devices. Therefore, efficient light trapping via reduction of light reflection is important for enhancing optical absorption. Figure 4(b) shows the measured surface reflection spectra of planar and textured β-Ga_2O_3 at a wavelength range of 200∼300 nm. The reflection of the planar surface was measured to be 41.3% at 200 nm and gradually decreased to 20.7% as the wavelength approached 300 nm. For the textured surface, the reflection was measured to be 28.8 and 6.5% at 200 and 300 nm, respectively. The reflection was reduced from 25.5% to 7.0% at 254 nm, as indicated by the dash line. The reduced reflection was attributed to the formation of the graded refractive index, considering that the dimension of the textured structure is smaller than the wavelength of incident light.[47]

Figure 5 shows the dark and photoresponse of the photodiodes fabricated on the planar and textured β-Ga_2O_3 surfaces at a bias range of −6 to 6 V. As shown in Fig. 5(a), the dark current (I_d) of the textured photodiode is increased compared to that of the photodiode on the planar surface in all bias regions except at zero bias. At −6 V, it increases to 1.58 nA from 0.015 nA at −6 V. We attribute the two orders of magnitude increase in I_d to the reduced SBH formed by the surface sub-oxide with a reduced band-gap.[44] Figure 5(b) shows the photocurrent (I_p) of the photodiodes characterized by a 254 nm UV lamp with a light intensity of 0.24 μW/cm^2. By comparing the planar with the textured photodiodes, there is a definitive enhancement observed. The I_p enhancement is ∼2–4 orders of magnitude across the entire bias range (Fig. S4). Figure 5(c) shows the calculated photoresponsivity based on the measured I_p and I_d, where the textured photodiode shows clear enhancement, compared to that of the planar photodiode. Specifically, the responsivity at −6 V increased from 1.3 to 71.7 A/W. We note, however, that the large degree of responsivity enhancement cannot be fully accounted for only by the absorption enhancement due to reduced reflection, implying the existence of a high internal gain in the textured photodiodes. Katz *et al.* reported high gain in Schottky barrier GaN UV detectors and attributed the gain to the surface states, which trap photogenerated minority carriers at the semiconductor-metal interface, inducing SBH lowering.[48] A high internal gain has also been reported in both β-Ga_2O_3 based Schottky barrier and MSM photodiodes.[49,50] We believe that the β-Ga_2O_x sub-oxide surface layer, with the reduced band-gap and SBH lowering due to I-MacEtch as described before, is responsible for the high internal gain observed from the textured β-Ga_2O_3 photodiodes.

Considering both dark current and photoresponsivity, the normalized photocurrent to dark current ratio (NPDR), $(I_p/I_d)/P_{inc}$, is an important figure of merit for MSM photodiodes and a larger value of this parameter indicates overall performance enhancement.[51,52] Figure 5(d) shows the extracted NPDR spectra. Although the mechanism of NPDR variation as a function of bias voltage is not understood at this point, the trend for the textured device for detecting 254 nm light is much flatter than its planar counterpart; importantly, as much as three orders of magnitude increase in NPDR was observed from the textured photodiode at the small bias range of −1 to 1 V. The ratio of NPDR between the planar and textured photodiode remained over 1 from −4 V all the way to 6 V. This indicates

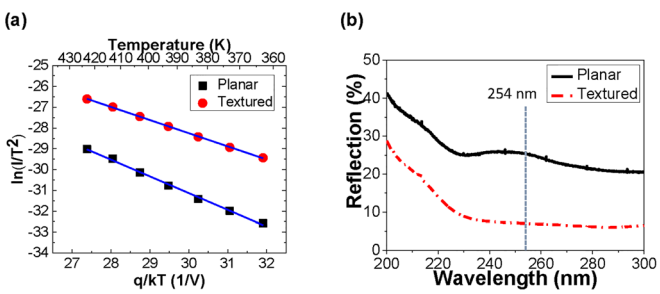

FIG. 4. (a) $ln(1/T^2)$ vs. q/kT plot of Pt/β-Ga_2O_3 Schottky diodes. The SBHs of the planar and textured Schottky diodes extracted are 1.49 and 1.36, respectively. (b) Measured surface reflection spectra of β-Ga_2O_3 before and after MacEtch texturing.

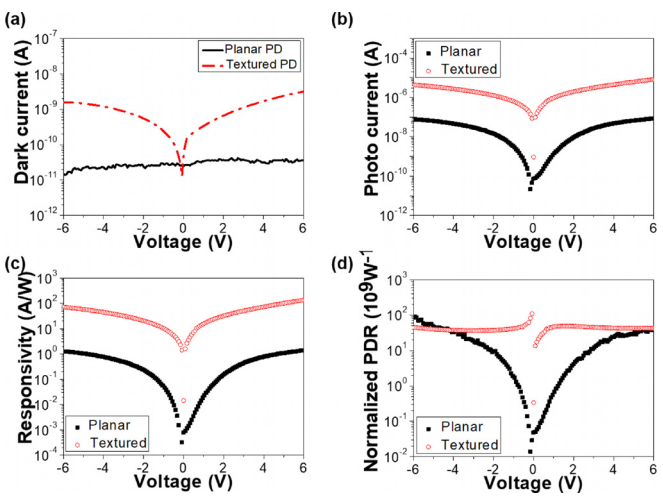

FIG. 5. Photodiode (PD) characterization as a function of bias voltage: (a) dark current, (b) photocurrent, (c) responsivity, and (d) NPDR of planar and textured PD, at 254 nm wavelength.

that the MacEtch-textured surface of β-Ga_2O_3 provides a competitive advantage over the planar surface for photodiode application in spite of an increased dark current.

In conclusion, we have reported the formation of the textured surface with nanoscale grooves in β-Ga_2O_3 using the UV photoenhanced I-MacEtch and its effect on the MSM photodiode performance. The textured surface has been determined to be sub-oxide caused by oxygen vacancies with a reduced band-gap energy from ~4.8 to ~4.1 eV as measured by XPS. MSM β-Ga_2O_3 photodiodes have been fabricated on the etched surfaces, showing enhanced photocurrent, I_p, and increased dark current, I_d, simultaneously, compared to the planar photodiodes. The increased I_d of the textured photodiodes is attributed to the reduced SBH as a result of the lower bandgap surface. The enhanced I_p results from the decreased surface reflection due to the texturing and high internal gain due to the SBH lowering. At 254 nm, the NPDR as a result of the surface texturing, shows clear enhancement over a wide bias range (from −4 V to 6 V), especially significant at a low bias range. This work demonstrates that the I-MacEtch method can achieve nanostructure-textured surfaces in β-Ga_2O_3 at room temperature without high energy reactive ions, for enhancing light absorption and engineering the surface properties in β-Ga_2O_3 optoelectronic applications.

See supplementary material for additional AFM image and histogram, XPS spectra, temperature dependent IV characteristics, and photocurrent plots and descriptions.

This material is based upon work supported by the U.S. Department of Energy, Office of Basic Energy Sciences, Division of Materials Sciences and Engineering under Award No. DE-FG0207ER46471 (chemical and structural characterization), Air Force Office of Scientific Research Grant No. FA9550-16-1-0010 (optical characterization), and the National Science Foundation under Grant Nos. #14-62946 and #18-09946 (etching and device fabrication).

[1]L. Sang, M. Liao, and M. Sumiya, Sensors **13**(8), 10482–10518 (2013).
[2]M. Kim, J.-H. Seo, U. Singisetti, and Z. Ma, J. Mater. Chem. C **5**(33), 8338–8354 (2017).
[3]T. Li, D. J. H. Lambert, A. L. Beck, C. J. Collins, B. Yang, M. M. Wong, U. Chowdhury, R. D. Dupuis, and J. C. Campbell, J. Electron. Mater. **30**, 872 (2001).
[4]K. B. Nam, J. Li, M. L. Nakarmi, J. Y. Lin, and H. X. Jiang, Appl. Phys. Lett. **84**, 5264 (2004).
[5]E. Cicek, R. McClintock, C. Y. Cho, B. Rahnema, and M. Razeghi, Appl. Phys. Lett. **103**, 181113 (2013).
[6]D.-S. Tsai, W.-C. Lien, D.-H. Lien, K.-M. Chen, M.-L. Tsai, D. G. Senesky, Y.-C. Yu, A. P. Pisano, and J.-H. He, Sci. Rep. **3**, 2628 (2013).
[7]M. Razeghi, Proc. IEEE **90**(6), 1006–1014 (2002).
[8]A. Soltani, H. A. Barkad, M. Mattalah, B. Benbakhti, J.-C. De Jaeger, Y. M. Chong, Y. S. Zou, W. J. Zhang, S. T. Lee, A. BenMoussa, B. Giordanengo, and J.-F. Hochedez, Appl. Phys. Lett. **92**, 053501 (2008).
[9]J. Xing, E. Guo, K.-J. Jin, H. Lu, J. Wen, and G. Yang, Opt. Lett. **34**(11), 1675–1677 (2009).
[10]L. Li, P. S. Lee, C. Yam, T. Zhai, X. Fang, M. Liao, Y. Koide, Y. Bando, and D. Golberg, Adv. Mater. **22**(45), 5145–5149 (2010).
[11]Y. Koide, M. Liao, and J. Alvarez, Diamond Relat. Mater. **15**(11–12), 1962–1966 (2006).
[12]M. Higashiwaki and G. H. Jessen, Appl. Phys. Lett. **112**, 060401 (2018).
[13]A. T. Neal, S. Mou, S. Rafique, H. Zhao, E. Ahmadi, J. S. Speck, K. T. Stevens, J. D. Blevins, D. B. Thomson, N. Moser, K. D. Chabak, and G. H. Jessen, Appl. Phys. Lett. **113**, 062101 (2018).
[14]D. Guo, Z. Wu, P. Li, Y. An, H. Liu, X. Guo, H. Yan, G. Wang, C. Sun, L. Li, and W. Tang, Opt. Mater. Express **4**(5), 1067–1076 (2014).
[15]T. Oshima, T. Okuno, N. Arai, N. Suzuki, S. Ohira, and S. Fujita, Appl. Phys. Express **1**(1), 011202-1-3 (2008).
[16]P. Feng, J. Y. Zhang, Q. H. Li, and T. H. Wang, Appl. Phys. Lett. **88**, 153107 (2006).
[17]S. Oh, J. Kim, F. Ren, S. J. Pearton, and J. Kim, J. Mater. Chem. C **4**, 9245–9250 (2016).
[18]Y. Li, J. Zhang, and B. Yang, Nano Today **5**(2), 117–127 (2010).
[19]Q. Zhou, D. C. Mclntosh, Y. Chen, W. Sun, Z. Li, and J. C. Campbell, Opt. Express **19**(24), 23664–23670 (2011).
[20]S.-I. Na, G.-Y. Ha, D.-S. Han, S.-S. Kim, J. Y. Kim, J.-H. Lim, D.-J. Kim, K.-I. Min, and S.-J. Park, IEEE Photonics Technol. Lett. **18**(14), 1512–1514 (2006).
[21]J. Yang, S. Ahn, F. Ren, R. Khanna, K. Bevlin, D. Geerpuram, S. J. Pearton, and A. Kuramata, Appl. Phys. Lett. **110**, 142101 (2017).
[22]J. Yang, F. Ren, R. Khanna, K. Bevlin, D. Geerpuram, L.-C. Tung, J. Lin, H. Jiang, J. Lee, E. Flitsiyan, L. Chernyak, S. J. Pearton, and A. Kuramata, J. Vac. Sci. Technol., B **35**, 051201 (2017).
[23]L. Zhang, A. Verma, H. Xing, and D. Jena, Jpn. J. Appl. Phys. Part 1 **56**, 030304 (2017).
[24]T. Oshima, T. Okuno, N. Arai, Y. Kobayashi, and S. Fujita, Jpn. J. Appl. Phys. Part 1 **48**, 040208 (2009).
[25]S. Ohira and N. Arai, Phys. Status Solidi C **5**, 3116 (2008).
[26]J. Son, Y. Kwon, J. Kim, and J. Kim, ECS J. Solid State Sci. Technol. **7**(8), Q148 (2018).
[27]X. Li and P. W. Bohn, Appl. Phys. Lett. **77**, 2572 (2000).
[28]X. Li, Curr. Opin. Solid State Mater. Sci. **16**(2), 71–81 (2012).
[29]J. Oh, H.-C. Yuan, and H. M. Branz, Nat. Nanotechnol. **7**(11), 743–748 (2012).
[30]M. Kim, S. Yi, J. D. Kim, X. Yin, J. Li, J. Bong, D. Liu, S.-C. Liu, A. Kvit, W. Zhou, X. Wang, Z. Yu, Z. Ma, and X. Li, ACS Nano **12**(7), 6748–6755 (2018).
[31]P. K. Mohseni, S. H. Kim, X. Zhao, K. Balasundaram, J. D. Kim, L. Pan, J. A. Rogers, J. J. Coleman, and X. Li, J. Appl. Phys. **114**, 064909 (2013).
[32]S. H. Kim, P. K. Mohseni, Y. Song, T. Ishihara, and X. Li, Nano Lett. **15**(1), 641–648 (2015).
[33]Y. Song, P. K. Mohseni, S. H. Kim, J. C. Shin, T. Ishihara, I. Adesida, and X. Li, IEEE Electron Device Lett. **37**(8), 970–973 (2016).
[34]L. Kong, Y. Song, J. D. Kim, L. Yu, D. Wasserman, W. K. Chim, S. Y. Chiam, and X. Li, ACS Nano **11**(10), 10193–10205 (2017).
[35]X. Li, Y.-W. Kim, P. W. Bohn, and I. Adesida, Appl. Phys. Lett. **80**, 980 (2002).
[36]T. L. Rittenhouse, P. W. Bohn, and I. Adesida, Solid State Commun. **126**(5), 245–250 (2003).
[37]J. A. Bardwell, J. B. Webb, H. Tang, J. Fraser, and S. Moisa, J. Appl. Phys. **89**, 4142 (2001).
[38]M. Kim, J.-H. Seo, D. Zhao, S.-C. Liu, K. Kim, K. Lim, W. Zhou, E. Waks, and Z. Ma, J. Mater. Chem. C **5**(2), 264–268 (2017).
[39]T. S. Wilhelm, Z. Wang, M. A. Baboli, J. Yan, S. F. Preble, and P. K. Mohseni, ACS Appl. Mater. Interfaces **10**(32), 27488–27497 (2018).
[40]T. S. Wilhelm, C. W. Soule, M. A. Baboli, C. J. O'Connell, and P. K. Mohseni, ACS Appl. Mater. Interfaces **10**(2), 2058–2066 (2018).
[41]K. Hanada, T. Moribayashi, T. Uematsu, S. Masuya, K. Koshi, K. Sasaki, A. Kuramata, O. Ueda, and M. Kasu, Jpn. J. Appl. Phys. Part 1 **55**, 030303 (2016).
[42]S. Miyazaki, Appl. Surf. Sci. **190**, 66–74 (2002).
[43]H. H. Tippins, Phys. Rev. **140**(1A), A316–A319 (1965).
[44]M. D. Heinemann, J. Berry, G. Teeter, T. Unold, and D. Ginley, Appl. Phys. Lett. **108**, 022107 (2016).
[45]D. Schroder, *Semiconductor Device and Material Characterization* (Wiley-Interscience, New York, 2006).
[46]Y. Yao, R. Gangireddy, J. Kim, K. K. Das, R. F. Davis, and L. M. Porter, J. Vac. Sci. Technol., B **35**, 03D113 (2017).
[47]W. H. Southwell, Opt. Lett. **8**(11), 584–586 (1983).
[48]O. Katz, V. Garber, B. Meyler, G. Bahir, and J. Salzman, Appl. Phys. Lett. **79**, 1417 (2001).
[49]R. Suzuki, S. Nakagomi, Y. Kokubun, N. Arai, and S. Ohira, Appl. Phys. Lett. **94**, 222102 (2009).
[50]D.-S. Wuu, S.-L. Ou, R.-H. Horng, P. Ravadgar, T.-Y. Wang, and H.-Y. Lee, Proc. SPIE **8263**, 826317 (2012).
[51]Z. Xia, H. Song, M. Kim, M. Zhou, T.-H. Chang, D. Liu, X. Yin, K. Xiong, H. Mi, X. Wang, F. Xia, Z. Yu, Z. Ma, and Q. Gan, Sci. Adv. **3**(7), e1602783 (2017).
[52]N. Youngblood, C. Chen, S. J. Koester, and M. Li, Nat. Photonics **9**, 247–252 (2015).